Electronic Supplementary Material (ESI) for ChemComm.

A tetrameric perylene diimide non-fullerene acceptor via unprecedented direct (hetero)arylation cross-coupling reaction

Abby-Jo Payne,[a] Jiali Song,[b] Yanming Sun[b] and Gregory C. Welch*[a]

[a]Department of Chemistry, University of Calgary
2500 University Drive NW Calgary, AB, Canada T2N 1N4

[b]School of Chemistry, Beihang University,
Beijing 100191, China. Email: sunym@buaa.edu.cn

* Corresponding Author
Email: gregory.welch@ucalgary.ca

SUPPORTING INFORMATION

Table of Contents

Materials and Methods

Materials: IDT core was purchased from Brilliant Matters and Silia*Cat*® DPP-Pd was received from SiliCycle. All remaining reagents were purchased from Sigma-Aldrich. All solvents and materials purchased were used without further purification.

Nuclear Magnetic Resonance (NMR): ^{1}H and $^{13}C\{^{1}H\}$ NMR spectra were recorded on a Bruker Avance-500 MHz spectrometer at 300 K. Chemical shifts are reported in parts per million (ppm). Multiplicities are reported as: singlet (s), doublet (d), triplet (t), multiplet (m), overlapping (ov), and broad (br).

High-resolution Mass Spectrometry (HRMS): High-resolution MALDI mass spectrometry measurements were performed courtesy of Jian Jun (Johnson) Li in the Chemical Instrumentation Facility at the University of Calgary. A Bruker Autoflex III Smartbeam MALDI-TOF (Na:YAG laser, 355nm), setting in positive reflective mode, was used to acquire spectra. Operation settings were all typical, e.g. laser offset 62-69; laser frequency 200Hz; and number of shots 300. The target used was Bruker MTP 384 ground steel plate target. Sample solution (~ 1 µg/mL in dichloromethane) was mixed with matrix trans-2-[3-(4-tert-Butylphenyl)-2-methyl-2-propenylidene]malononitrile (DCTB) solution (~ 5mg/mL in methanol). Pipetted 1µl solution above to target spot and dried in the fume hood.

Elemental Analysis (CHN): Elemental analysis was performed courtesy of Jian Jun (Johnson) Li in the Chemical Instrumentation Facility at the University of Calgary. All samples were run in duplicate on a Perkin Elmer 2400 Series II CHN Analyzer.

Cyclic Voltammetry (CV): All electrochemical measurements were performed using a Model 1200B Series Handheld Potentiostat by CH Instruments Inc. equipped with Ag wire, Pt wire, and glassy carbon electrode, as the pseudo reference, counter electrode, and working electrode, respectively. Glassy carbon electrodes were polished with alumina. The cyclic voltammetry experiments were performed in anhydrous dichloromethane solution with ~0.1 M tetrabutylammonium hexafluorophosphate ($TBAPF_6$) as the supporting electrolyte at scan rate 100 mV/s. All electrochemical solutions were purged with dry N_2 for 5 minutes to deoxygenate the system. Solution CV measurements were carried out with a small molecule concentration of ~0.5 mg/mL in dichloromethane. The ionization potentials (IP) and electron affinities (EA) were estimated by correlating the onsets (E_{ox}Fc/Fc+, E_{red}Fc/Fc+) to the normal hydrogen electrode (NHE), assuming the IP of Fc/Fc+ to be 4.80 eV.[1]

UV-Visible Spectroscopy (UV-Vis): All absorption measurements were recorded using Agilent Technologies Cary 60 UV-Vis spectrometer at room temperature. All solution UV-Vis spectroscopy experiments were run in $CHCl_3$ using 10 mm quartz cuvettes. Neat films were prepared by spin-coating 0.1 mL from a 1 % wt/v solution ($CHCl_3$) onto clean onto Corning glass micro slides. Prior to use, glass slides were cleaned with soap and water, acetone and isopropanol, and followed by UV/ozone treatment using a Novascan UV/ozone cleaning system.

Photoluminescence (PL): All emission measurements were recorded using an Agilent Technologies Cary Eclipse fluorescence spectrophotometer at room temperature. Thin-films were

prepared by spin-coating 1 % wt/v solutions from $CHCl_3$ on Corning glass micro slides. Prior to use, glass slides were cleaned with soap and water, and acetone and isopropanol, and followed by UV/ozone treatment using a Novascan UV/ozone cleaning system.

Computational details: Gas-phase B3LYP/6-31G(d,p) ground-state equilibrium geometry optimizations were considered within Gaussian 09[2]. In order to reduce the computational cost while still accounting for the electron-donating ability of the substituent, the solubilizing chains along the conjugated backbone of IDT-$NPDI_4$ were truncated in all calculations to methyl groups. The dihedral angles that control the relative orientation of the π-systems were systematically altered for these four structures to help ensure that lower energy minima were not missed, where each resulting structure was characterized through frequency calculations at the same level of theory.

Experimental

Synthesis of PDI precursor (NPDI-Br)

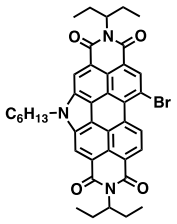

The brominated N-annulated PDI precursor was synthesized as previously reported.[3]

IDT

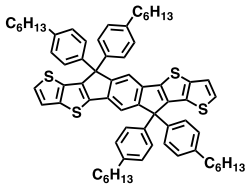

The IDT core was purchased from Brilliant Materials.

Note reaction A in Scheme 1 was repeated three times with the same results observed each time.

Synthesis of IDT-NPDI$_4$

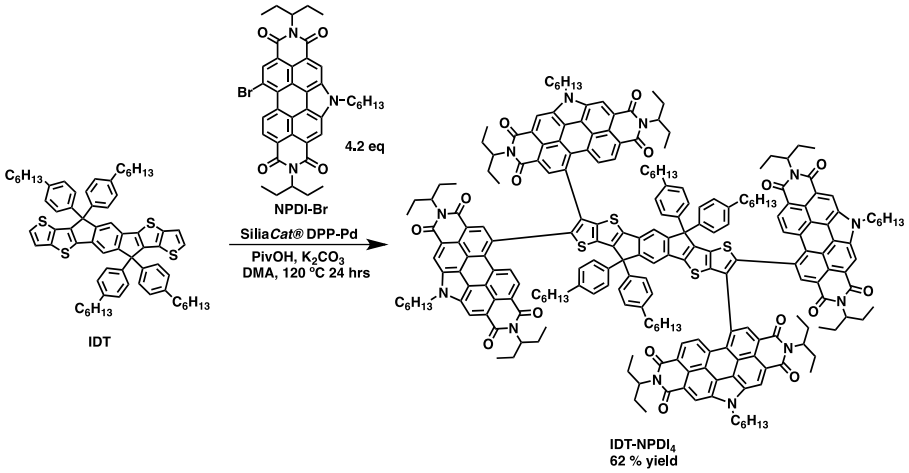

In a 5 mL pressure vial, IDT (0.100 g, 0.098 mmol, 1eq), PDI (0.293 g, 0.41 mmol, 4.2 eq), Silia*Cat*® DPP-Pd (5 mol % Pd to IDT*4), pivalic acid (30 mol % to IDT), and potassium carbonate (0.061 g, 0.44 mmol, 4.5 eq.) were added with a stir bar followed by the addition of anhydrous *N,N'*-dimethylacetamide (4 mL). The reaction mixture was sealed with a Teflon® cap under N_2 and heated at 120 °C in a LabArmor® bead bath for 24 hours. After 24 hours, the reaction

mixture was poured into acetone (50 mL) and stirred overnight. The precipitated product was collected by filtration and the filtrate was discarded. The solid product was subsequently dissolved in dichloromethane and sent through a short neutral alumina plug to remove the silica-supported catalyst and any remaining inorganics. Upon removal of solvent, the resulting material was sonicated in EtOAc (50 mL) before allowing it to stir at reflux for several hours. The resulting solution was allowed to cool to room temperature and the resulting material was subsequently filtered washing with EtOAc followed by acetone and isolated as a dark red powder yielding the desired product in 70 % yield (0.242 g, 0.068 mmol, 70 % yield).

^{1}H NMR (500 MHz, $CDCl_3$, ppm): δ 9.10 (s, br, 1H, PDI), 9.07 (s, br, 1H, PDI), 9.00 (s, br, 1H, PDI), 8.96 (s, br, 1H, PDI), 8.68-8.76 (m, 1H, PDI), 8.58-8.68 (m, 2H, PDI), 8.55 (s, br, 1H, PDI), 8.42-8.52 (m, 2H, PDI), 7.37 (s, 1H, IDT), 7.20 (d, *J*= 8.2 Hz, 2H, IDT), 7.17 (d, *J*= 7.8 Hz, 2H, IDT), 7.10 (t, 4H, IDT), 5.19-5.30 (m, 2H, PDI), 4.86-4.97 (m, ov, 4H, PDI), 4.63-4.79 (m, 2H, PDI), 2.57 (t, br, 4H, IDT), 2.32-2.47 (m, 6H, PDI), 2.26-2.13 (m, 6H, PDI), 2.09-1.91 (m, 6H, PDI), 1.83-1.66 (m, 4H), 1.62-1.56 (m, 4H, IDT), 1.17-1.48 (m, ov, 24H, IDT/PDI), 0.97-1.09 (m, 12H, PDI), 0.76-0.88 (m, ov, 16H, IDT/PDI), 0.44-0.66 (m, 6H).

^{13}C NMR (500 MHz, $CDCl_3$, ppm): δ 152.92, 146.81, 143.77, 141.73, 141.66, 141.40, 139.34, 138.86, 138.66, 135.48, 134.44, 134.32, 134.25, 132.60, 132.32, 132.10, 132.00, 131.95, 131.78, 131.11, 128.37, 128.15, 128.12, 127.31, 127.09, 124.44, 124.42, 124.11, 124.03, 122.64, 122.57, 122.38, 122.33, 119.25, 119.17, 119.13, 116.82, 62.63, 57.16, 56.87, 46.38, 35.01, 34.79, 31.09, 30.98, 30.92, 30.82, 30.78, 30.63, 30.50, 28.62, 28.57, 26.32, 26.29, 24.68, 24.26, 22.01, 21.90, 21.88, 13.51, 13.43, 13.41, 13.38, 10.92, 10.88, 10.63, 10.62, 10.59.

Tabulated aromatic peaks: 37; Tabulated aliphatic peaks: 31

MS (MALDI-TOF): Calculated: 3520.19; Found: 3519.64.

Elemental Analysis (EA): Theoretical: C= 77.74 %, H= 6.58 %, N= 4.77 %; Found: C= 77.38 %, H= 6.50 %, N= 4.79 %

Solution NMR spectra

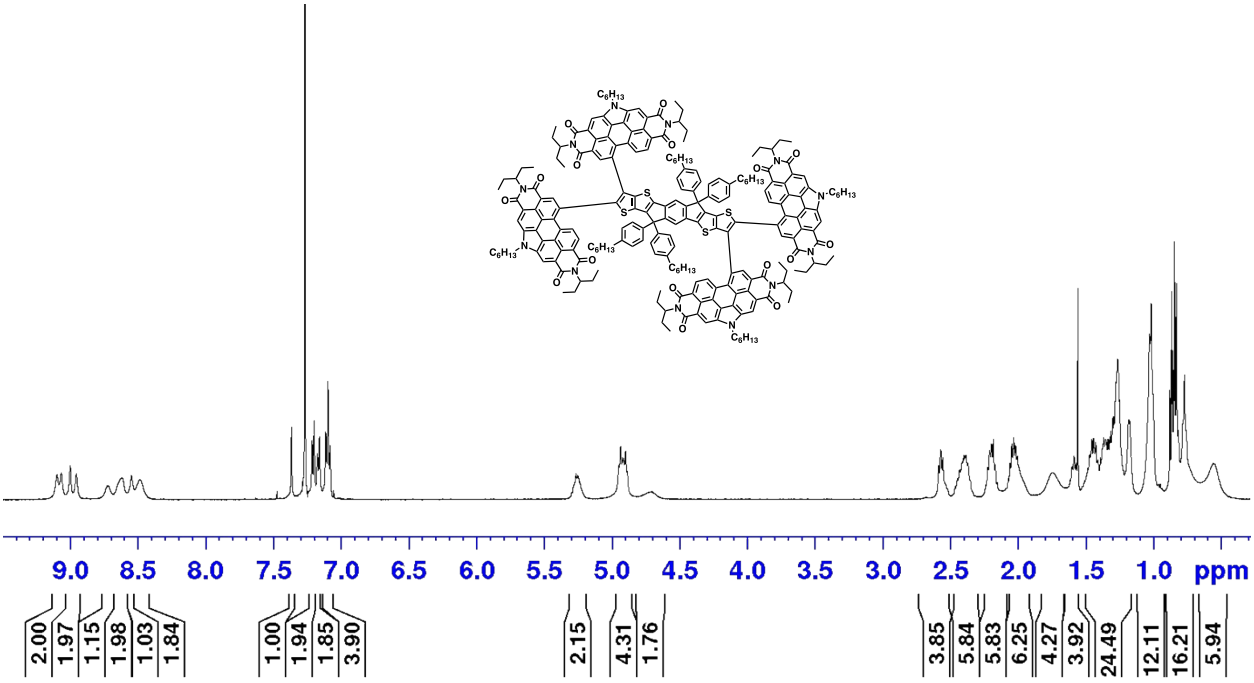

Figure S1. ^{1}H NMR spectrum of IDT-NPDI$_4$ in $CDCl_3$

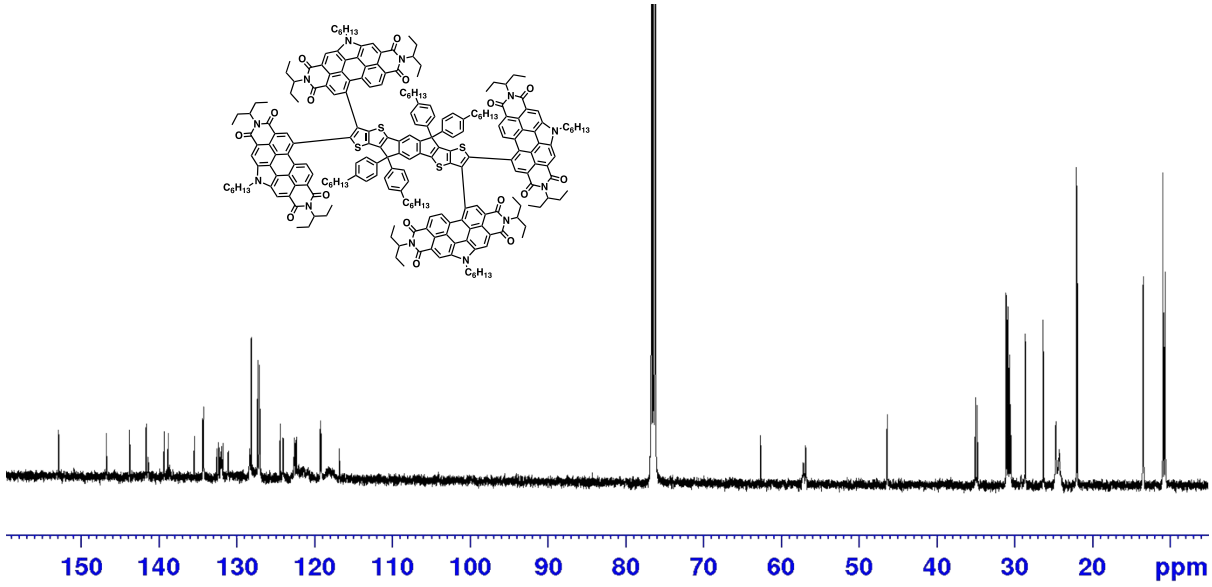

Figure S2. ^{13}C NMR spectrum of IDT-NPDI$_4$ in $CDCl_3$

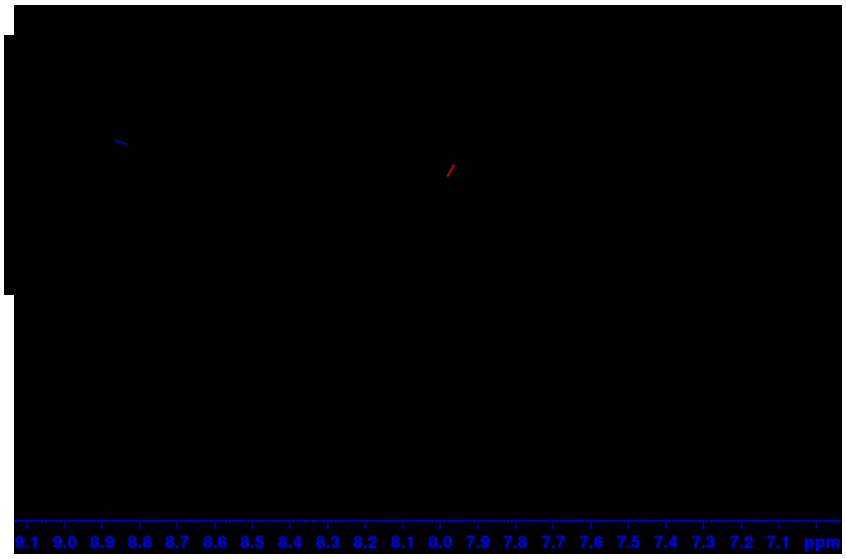

Figure S3. Solution ^{1}H NMR spectrum (aromatic region) of mono-substituted fraction from reaction **B** as confirmed by MALDI-TOF mass spectrometry (Figure S7; *m/z* 1643.77; exact mass 1643.76).

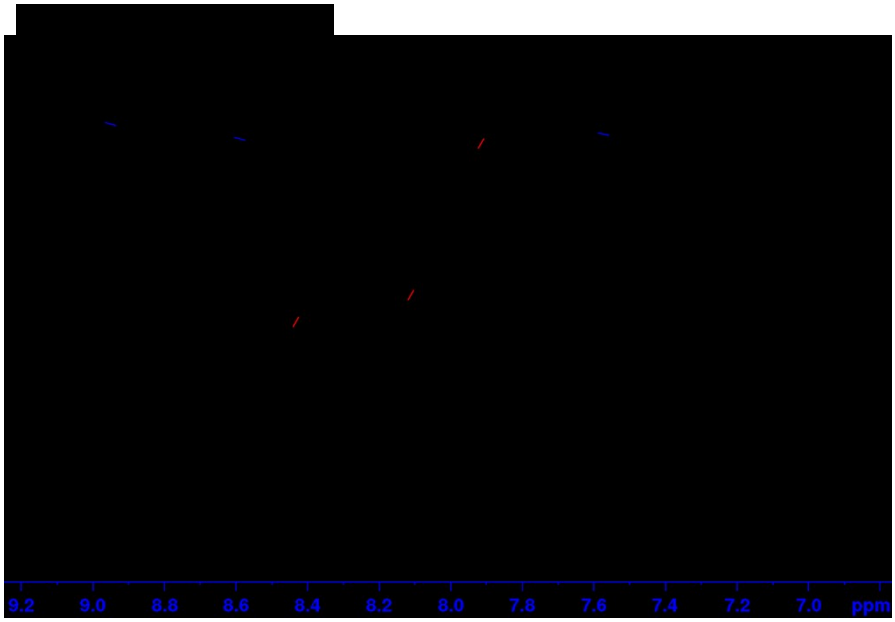

Figure S4. Solution ^{1}H NMR spectrum (aromatic region) of bis-substituted fraction from reaction **B** as confirmed by MALDI-TOF mass spectrometry (Figure S8; *m/z* 2269.05; exact mass 2269.06).

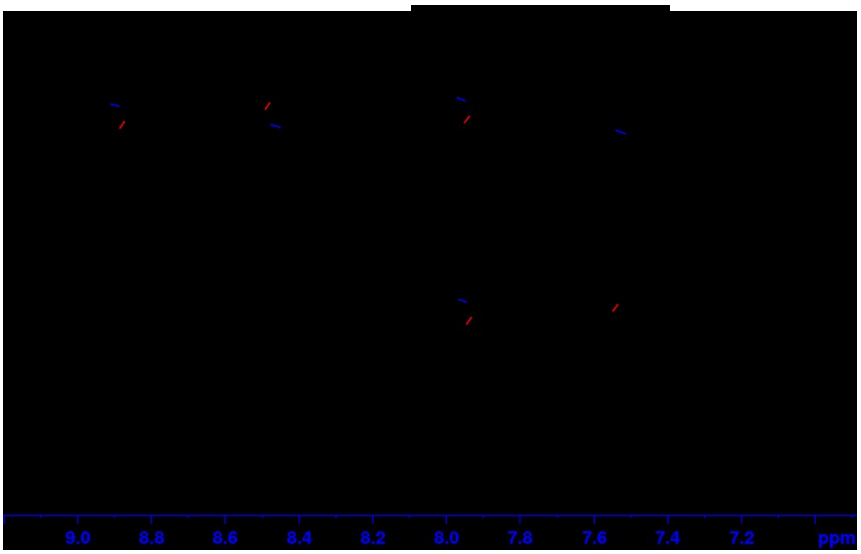

Figure S5. Solution ^{1}H NMR spectrum (aromatic region) of a mixture of tris and tetra-substituted fraction from reaction **B** as confirmed by MALDI-TOF mass spectrometry (Figure S9; *m/z* 2897.24; nominal mass 2896.84, *m/z* 3523.70; nominal mass 3522.60.

Maldi-TOF mass spectra

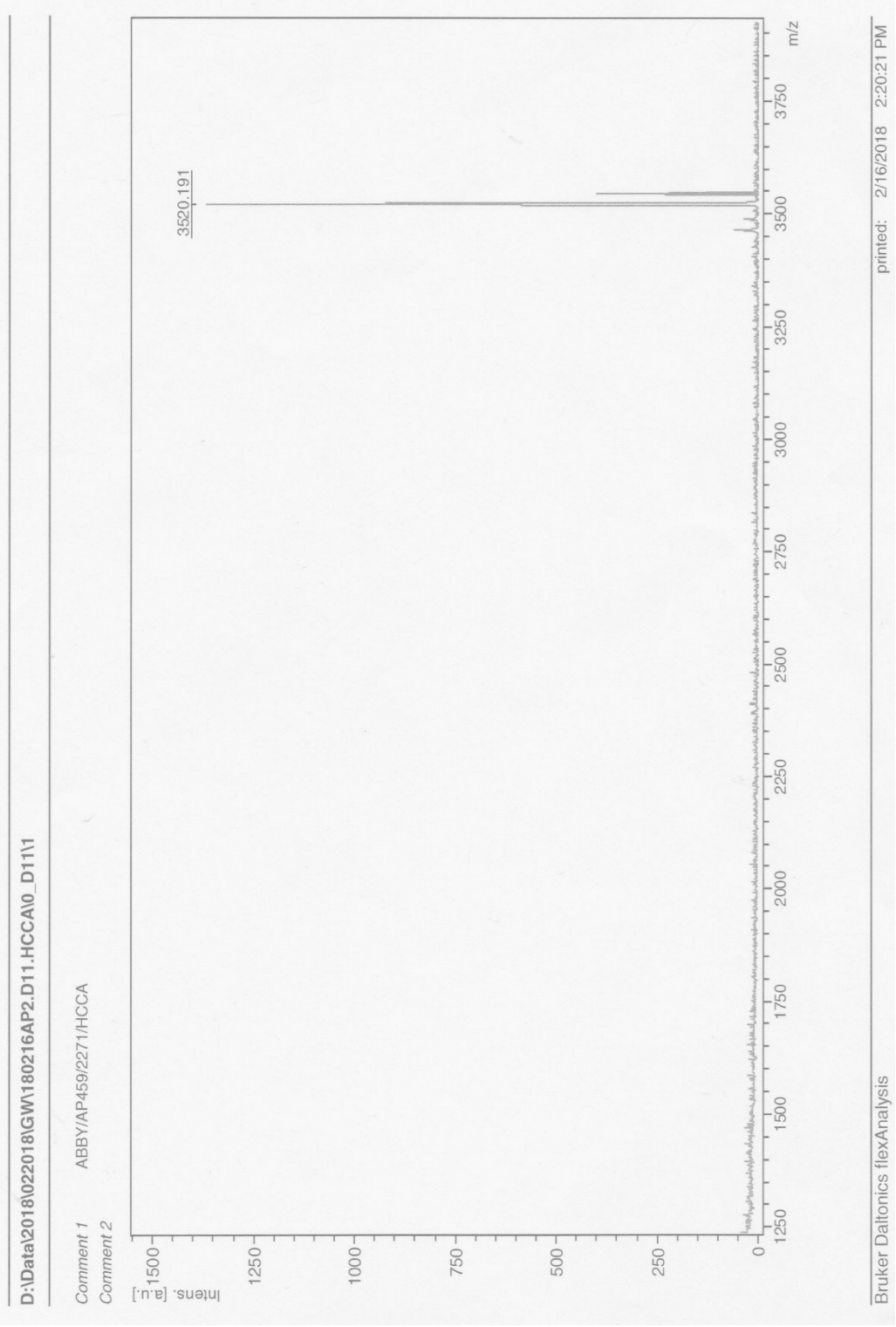

Figure S6. MALDI-TOF mass spectrum of IDT-$NPDI_4$.

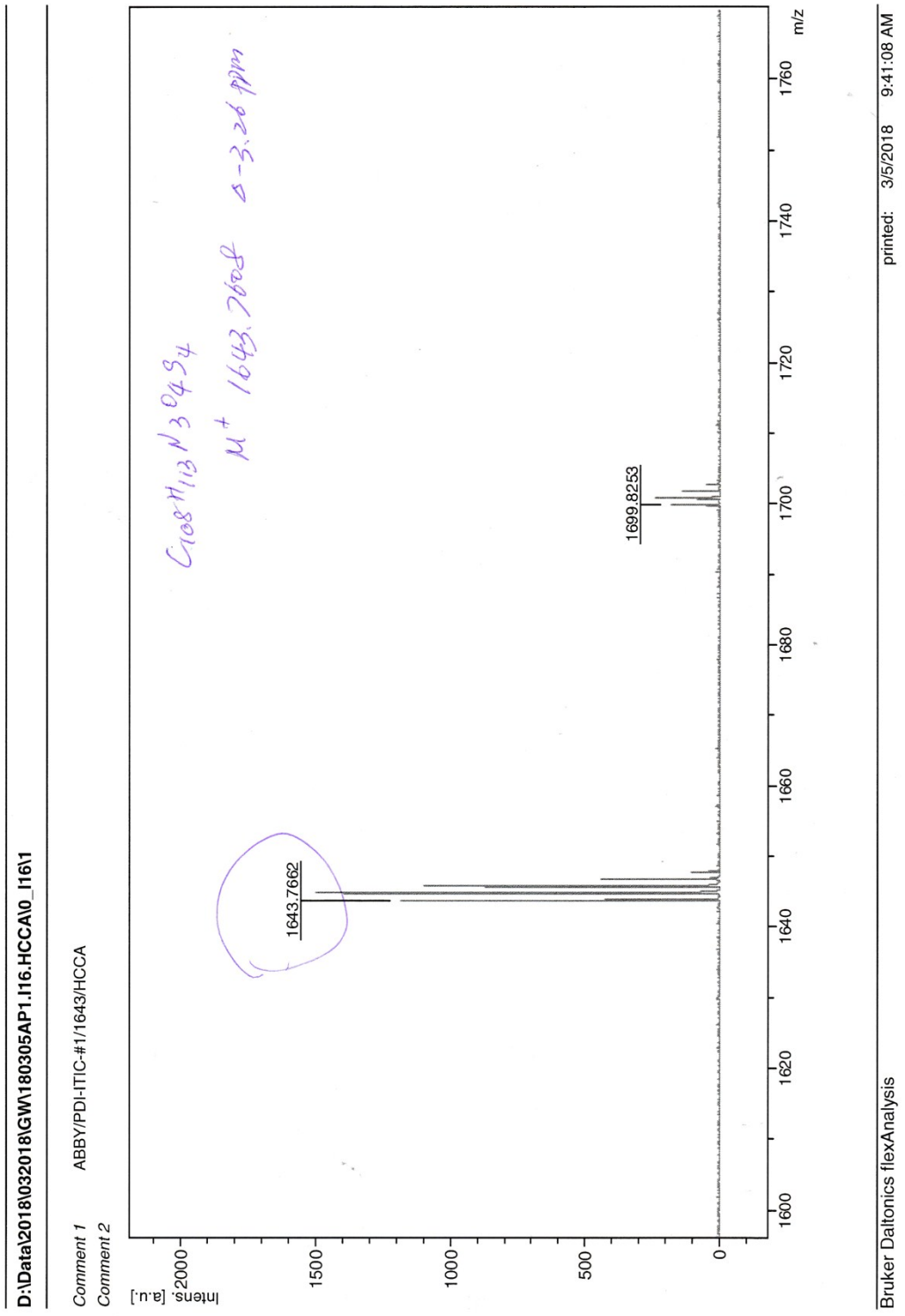

Figure S7. MALDI-TOF mass spectrum of mono-substituted fraction from reaction **B** (IDT-NPDI).

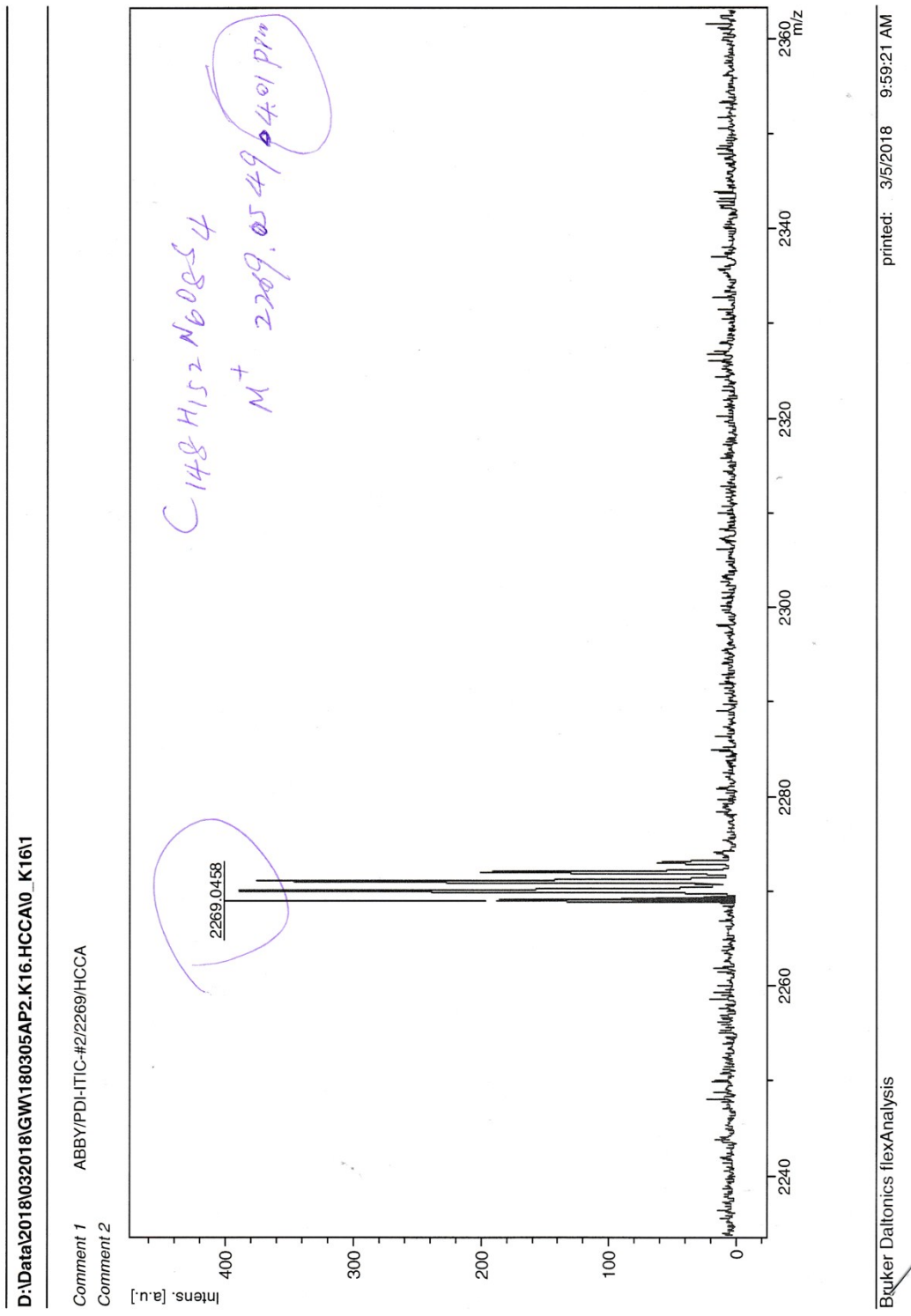

Figure S8. MALDI-TOF mass spectrum of bis-substituted fraction from reaction **B** (IDT-$NPDI_2$).

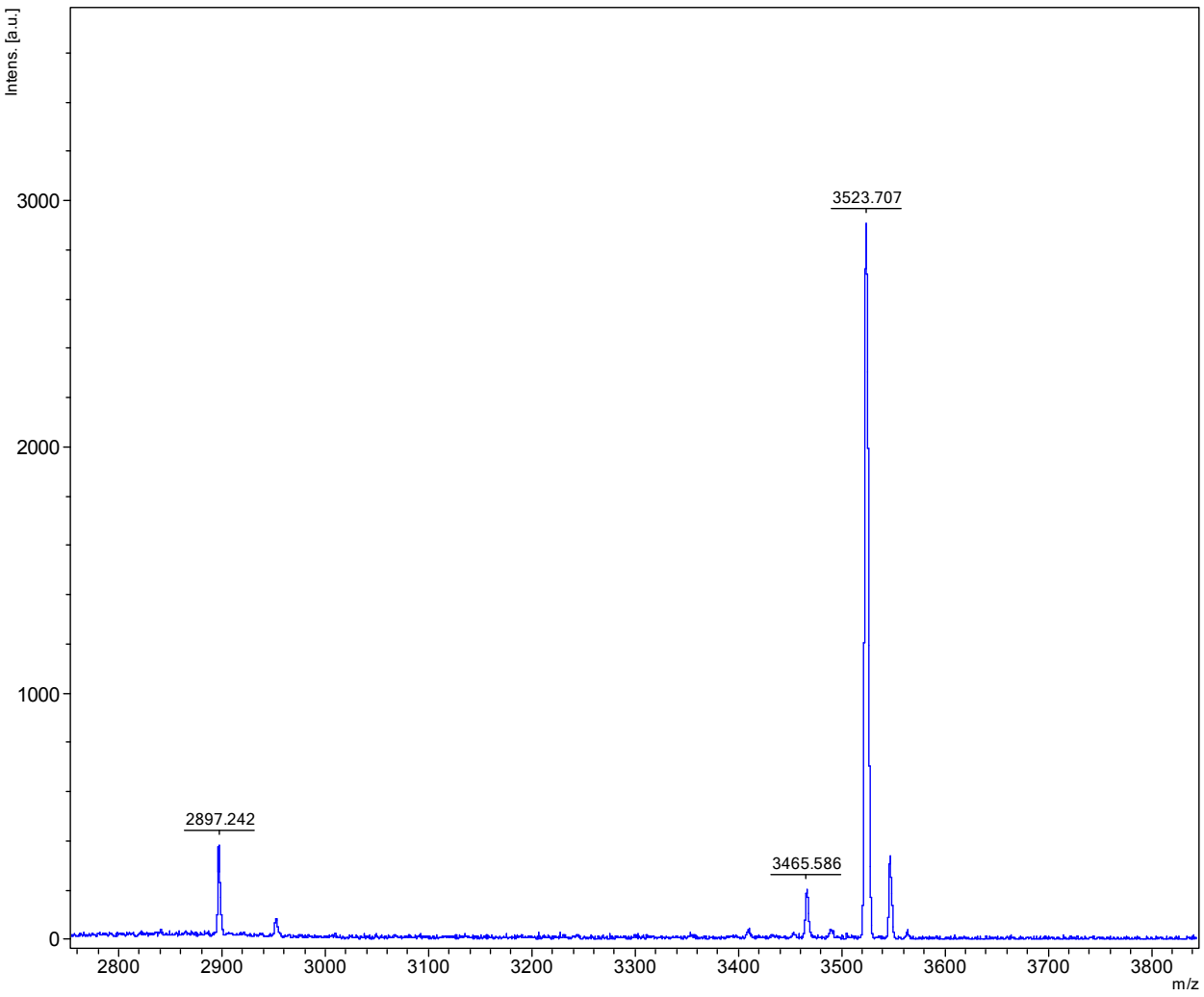

Figure S9. MALDI-TOF mass spectrum of mixed tris/tetra-substituted fraction from reaction **B** (IDT-NPDI$_3$ and IDT-NPDI$_4$).

Elemental Analysis

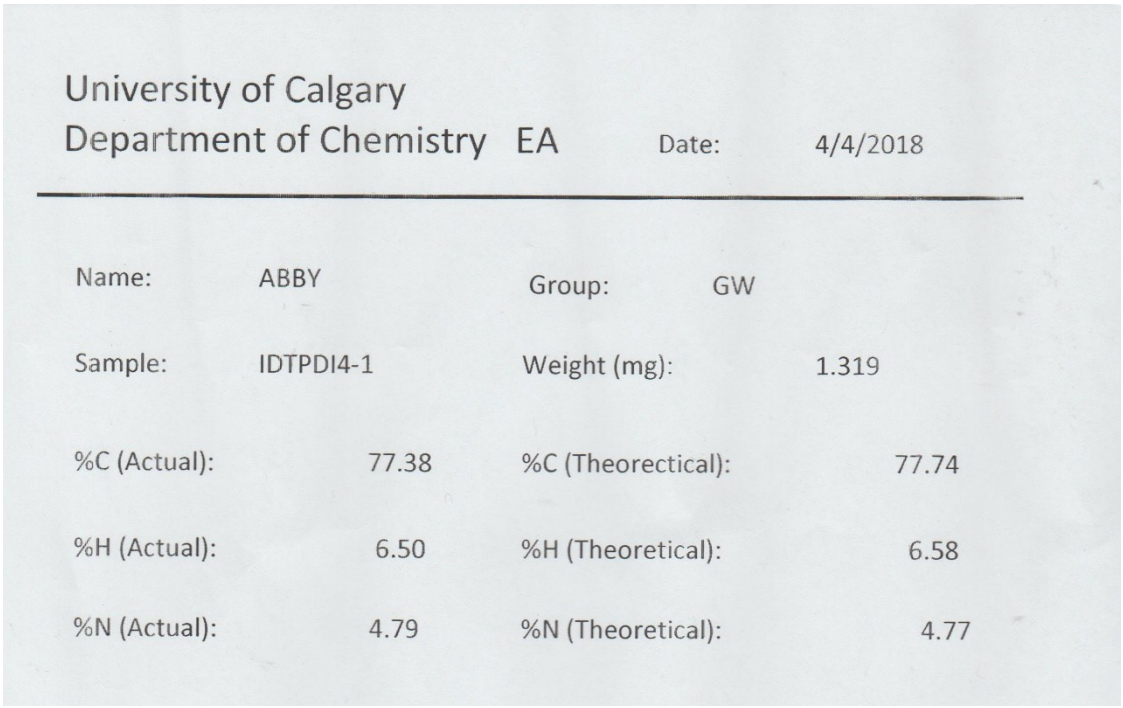

University of Calgary
Department of Chemistry EA Date: 4/4/2018

Name:	ABBY	Group:	GW
Sample:	IDTPDI4-1	Weight (mg):	1.319
%C (Actual):	77.38	%C (Theorectical):	77.74
%H (Actual):	6.50	%H (Theoretical):	6.58
%N (Actual):	4.79	%N (Theoretical):	4.77

Figure S10. EA results of IDT-NPDI$_4$.

Optical Characterization

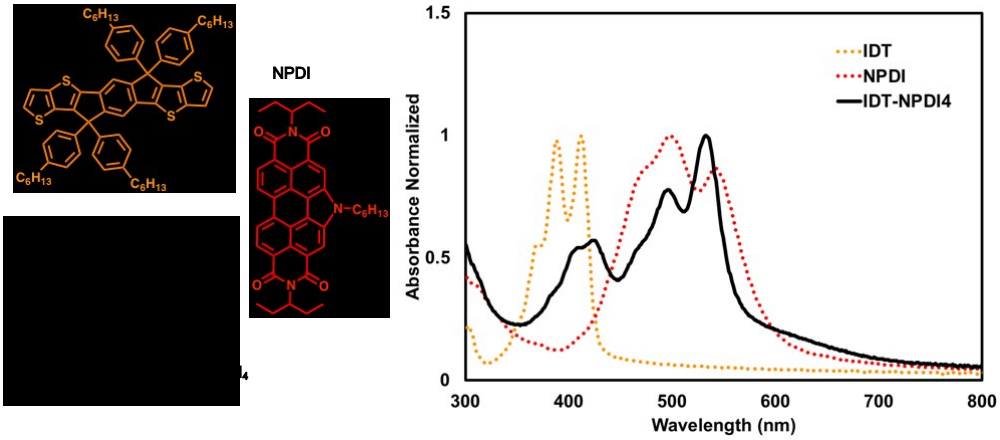

Figure S11. Normalized thin film ($CHCl_3$) absorption profiles of IDT (orange dotted trace), NPDI (red dotted trace), and IDT-$NPDI_4$ (solid black trace).

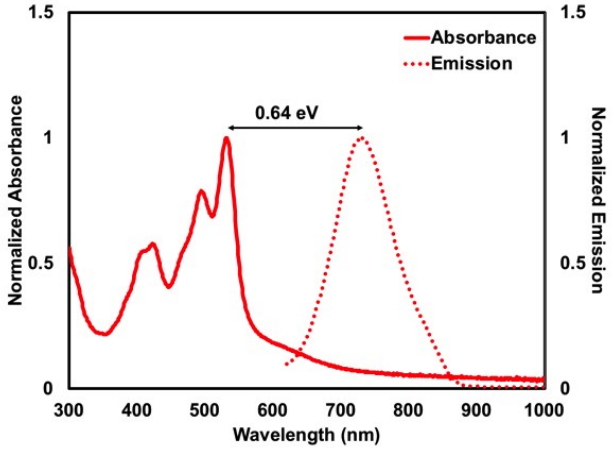

Figure S12. Normalized thin film ($CHCl_3$) absorption (solid trace) vs. emission (dotted trace) of IDT-$NPDI_4$.

Organic Solar Cell Devices

Device Fabrication and Testing

Organic solar cells with an inverted device architecture of ITO/ZnO/BHJ/MoO_3/Ag were fabricated. The ITO-coated glass substrates were cleaned by ultrasonic treatment in detergent deionized water, acetone and isopropyl alcohol for 20 minutes, respectively. ZnO precursor solution was spin-coated on top of the ITO at 4000 rpm and then the film was annealed at 200 °C for 15 min in air. The BHJ layers were spin-coated at 1700 rpm from a solution of PTB7-Th: IDT-$NPDI_4$ with weight ratio of 1:1 in chlorobenzene (CB) with a total concentration of 20 mg/mL. Chloronaphthalene (CN) was used as the solvent additive. Mixed solutions with different CN amounts were stirred overnight prior to casting. The BHJ layers were heated at 100 °C for 10 min in a N_2-filled glovebox to remove excess solvent. The MoO_3 were deposited by sequential thermal evaporation of 3 nm followed by 90 nm of Ag. Current density-voltage (J-V) characteristics were measured using a Keithley 2400 Source Measure Unit. The currents were measured under 100 mW/cm^2 simulated 1.5 Global (AM 1.5 G) solar simulator (Enli Technology Co., Ltd, SS-F5-3A). The light intensity was calibrated by a standard Si solar cell (SRC-2020, Enli Technology Co., Ltd). EQE spectra were carried out by using a QEX10 Solar Cell IPCE measurement system (PV Measurements, Inc.). Atomic force microscopy (AFM) measurements were carried out using a Dimension Icon AFM (Bruker) in the tapping mode.

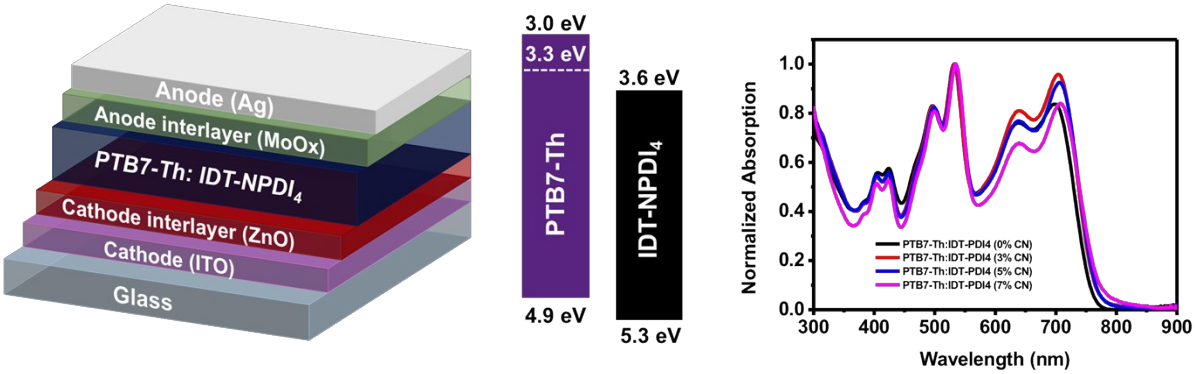

Figure S13. Solar cell device architecture (left) and energy levels of active layer materials (middle). Energy levels estimated from solution cyclic voltammetry measurements (black) or from the onset of absorption (white) by subtracting from the ionization potential determined by cyclic voltammetry. Absorption profiles of active layers processed with and without CN additive (right).

SCLC Measurements

The charge transport properties were evaluated *via* the space charge limited current (SCLC) method. The electron-only devices were fabricated with a structure of ITO/ZnO/photoactive layer/ZrAcac/Al, and the hole-only devices are fabricated with a structure of ITO/PEDOT:PSS/BHJ/Ag. BHJ active layer was spin-cast as described above, using 5% v/v/ CN additive. The *J*–V curves of devices were fitted by using the Mott–Gurney equation: $J = 9\varepsilon_o\varepsilon_r\mu V^2/8L^3$, where J is the current density, ε_0 is the permittivity of free space, ε_r is the permittivity

of the active layer, μ is the hole mobility or electron mobility, V is the internal voltage of the device ($V = V_{appl} - V_{bi}$), where V_{app} is the applied voltage, V_{bi} is the offset voltage (V_{bi} is 0 V here), and L is the film thickness of the active layer. The electron mobility or hole mobility was calculated from the slope of the SCLC curve.

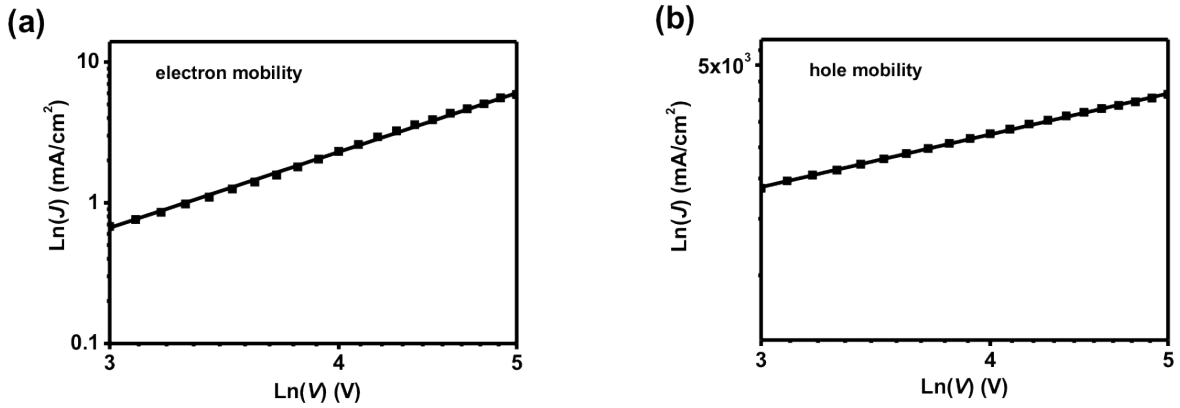

Figure S14. Space charge limited current (SCLC) measurement plots. (a) electron mobility and (b) hole mobility.

Table S1. Space charge limited current (SCLC) tabulated data.

Sample	Electron mobility ($cm^2V^{-1}s^{-1}$)	Hole mobility ($cm^2V^{-1}s^{-1}$)	The ratio of hole and electron mobility
PTB7-Th:IDT-$NPDI_4$	4.00×10^{-6}	2.74×10^{-4}	68.5

References

1 J. Pommerehne, H. Vestweber, W. Guss, R. F. Mahrt, H. Bässler, M. Porsch and J. Daub, *Adv. Mater.*, 1995, **7**, 551–554.

2 M. Frisch, G. Trucks, H. Schlegel, G. Scuseria, M. Robb, J. Cheeseman, G. Scalmani, V. Barone, B. Mennucci, G. Petersson, H. Nakatsuji, M. Caricato, X. Li, H. Hratchian, A. Izmaylov, J. Bloino, G. Zheng, J. Sonnenberg, M. Hada, M. Ehara, K. Toyota, R. Fukuda, J. Hasegawa, M. Ishida, T. Nakajima, Y. Honda, O. Kitao, H. Nakai, T. Vreven, J. Montgomery, J. Peralta, F. Ogliaro, M. Bearpark, J. Heyd, E. Brothers, K. Kudin, V. Staroverov, R. Kobayashi, J. Normand, K. Raghavachari, A. Rendell, J. Burant, S. Iyengar, J. Tomasi, M. Cossi, N. Rega, J. Millam, M. Klene, J. Knox, J. Cross, V. Bakken, C. Adamo, J. Jaramillo, R. Gomperts, R. Stratmann, O. Yazyev, A. Austin, R. Cammi, C. Pomelli, J. Ochterski, R. Martin, K. Morokuma, V. Zakrzewski, G. Voth, P. Salvador, J. Dannenberg, S. Dapprich, A. Daniels, Farkas, J. Foresman, J. Ortiz, J. Cioslowski and D. Fox, *Gaussian 09 Revis. E01 Gaussian Inc Wallingford CT*.

3 A. D. Hendsbee, J.-P. Sun, W. K. Law, H. Yan, I. G. Hill, D. M. Spasyuk and G. C. Welch, *Chem. Mater.*, 2016, **28**, 7098–7109.